Modeling plasma actuators with air chemistry for effective flow control

Kunwar Pal Singh and Subrata Roy[a)]
Computational Plasma Dynamics Laboratory and Test Facility, Mechanical and Aerospace Engineering, University of Florida, Gainesville, Florida 32611-6300

(Received 26 February 2007; accepted 10 May 2007; published online 29 June 2007)

An asymmetric dielectric barrier discharge model is presented for real gas air chemistry using a self-consistent multibody system of plasma, dielectric, and neutral gas modeled together to predict the electrodynamic force imparted to the working gas. The equations governing the motion of charged and neutral species are solved with Poisson equation using finite element method using a Galerkin weak formulation. Electric field profile changes with the increase in grounded electrode and the density increases downstream. The electrodynamic force development mechanism is studied over a flat plate due to charge and neutral species production from adjacent air in a radio frequency driven barrier discharge. The time average of the force shows mostly acceleration above the actuator. Numerical simulation confirms that the magnitude of force increases very slightly with the increase in the length of grounded electrode. © *2007 American Institute of Physics*.
[DOI: 10.1063/1.2749467]

I. INTRODUCTION

Electrodynamic modifications of air flowing around flat plates and air craft wings have been documented both experimentally and numerically.[1–3] These are primarily surface barrier discharges using asymmetric configurations of electrode sets. The symmetric configuration of electrode sets can produce flow oscillation similar to synthetic jets. For plasma actuators with spatially displaced electrodes the airflow inducement is close to the dielectric surface with a time averaged flow velocity measured between 1 and 3 m/s. These actuators exhibit several benefits in active flow control applications, including absence of moving parts, rapid on-off deployment, and attractive self-limiting characteristics. The discharge may be characterized as transient with a time scale of the order of a few microseconds while that for the bulk gas flow is in milliseconds. This allows the fluid to respond relatively instantaneously to the electrical inputs. Experimental study and numerical predictions on the effect of different discharge parameters such as applied voltage wave form, distance between electrodes, dielectric thickness, and permittivity are documented by various researchers.[4,5] These results show that the volumetric body force increases as a function of frequency and applied voltage. The parametric relationship is not clear and is an area of continued investigation. Also the nature of the plasma gas interaction is not well understood. Acoustic measurements of the dielectric barrier discharge (DBD) plasma actuator[6] suggest that compressibility effects may contribute in the momentum coupling between plasma and neutral gas. Specific modality of discharge whether it is glow, Townsend, or streamers will help determine how the body force is transported from charge to neutral species. The effect of this body force in controlling three-dimensional laminar and transitional flow structures has been studied utilizing both phenomenological and first-principles models.

Phenomenological and circuit based models have shown some success in mimicking overall electrical characteristic of the discharge but are fundamentally limited from inherent static and/or predetermined charge imposition.[7] The first-principles models suitable for capturing detailed dynamics are also computationally challenging. For example, the surface barrier discharge in these actuators consists of repeated burst of microdischarges which appears as an optical glow due to nanosecond time scales. Resolution of a typical microdischarge driven by electron decay requires running simulation at a time scale of picoseconds or lower, thus imposes practical restriction to ever reaching the fluid time scale which is in milliseconds. Recent development of a loosely coupled fluid plasma formulation[5,8] has shown reasonable success in describing radio frequency (rf) powered electrohydrodynamic (EHD) control of NACA wing stall, laminar separation over a ramp, boundary layer transition on a flat plate, and turbulent separation over a wall-mounted hump. The plasma equations are based on a self-consistent simulation of charge species continuity and electric field equations. Once the reasonable periodicity is achieved in plasma characteristic, the temporally resolved EHD force is employed into the fluid equations to predict the effect of plasma in flow actuation. Interestingly, for moderate Reynolds numbers either coflow or counterflow pulsed actuators with sufficiently high frequency (kHz) were found to mitigate wing stall.[9] Unsteady flow actuation with a duty factor seemed to perform better than continuous operation of the rf plasma actuator. These results underscore the importance of accurately resolving the unsteady body force and understanding its transition and turbulence enhancement mechanisms for effective plasma actuation.

Numerical simulations of an asymmetrically arranged DBD actuator employing multispecies hydrodynamics[5] and particle-in-cell and direct Monte Carlo (PIC-DSMC) methods[10] by independent research groups have found that ionization is not equal during positive and negative parts of the alternating cycle producing a net force in one direction.

[a)]Electronic mail: roy@ufl.edu

Recently, the dc corona discharges and ac dielectric barrier discharges have been investigated under a range of operating conditions. Adjustment of the actuator geometry, dielectric materials, power frequency, and rms voltage shows improvement in power transferred to the neutral gas flow by ion-neutral collisions. Also power losses due to inadequate impedance matching of the power supply to the actuator, dielectric heating, and power required to maintain the atmospheric pressure plasma have been reduced for better performance of actuator.[4]

In our earlier work, we have shown that electron deposition downstream of the overlap region of the electrodes results in formation of virtual negative electrode which always attracts the ions. The force on the charge separation is in the positive x direction during most of the positive half of the rf voltage and in the negative x direction during most of the negative half of the rf voltage. The magnitude of the former force is higher than the latter. Thus, domain integration of the force on the charge separation and time average of the force was found primarily to be in the positive x and negative y directions. We solved the equations governing dynamics of electrons, ions, and fluid to obtain spatiotemporal profiles of electron density, ion density, electric potential, neutral gas density, and neutral gas velocity. We documented how the EHD force is controlled by the dielectric characteristics, applied voltage, frequency, the asymmetric configuration of the electrodes, and thickness of the exposed electrode. Additionally, we utilized the force field calculated from the first principles[5] to predict the effect of increasing number of electrodes on the wall jet while the electrodes are kept at a single phase and at a phase gap. The momentum transfer to the gas was also predicted for varying the distance between the powered electrodes.

Recently we have presented a real gas model with airlike N_2/O_2 mixture and have shown preliminary results.[11] In this paper, we summarize our recent developments with the atmospheric barrier discharge model for eight species of airlike medium and the generated EHD force interactions over a flat dielectric. This paper is organized as follows: Sec. II describes geometry of the plasma actuator, the problem statement and air chemistry is given in Sec. III, initial conditions and boundary conditions are given in Sec. IV, computed results and discussion are given in Sec. V, and finally Sec. VI summarizes the conclusions.

II. GEOMETRY DESCRIPTION

Figure 1 shows schematic of an asymmetric single dielectric barrier plasma actuator. It consists of two electrodes separated by a dielectric. The upper electrode is exposed to the air while the lower electrode is placed underneath the dielectric. The region simulated is 4 cm long and 1 cm high. The lower part of the domain consists of a 0.1 cm thick insulator with relative dielectric constant $\varepsilon_r=10$ while the upper part is filled with air of relative dielectric constant $\varepsilon_r=1.0055$. We have assumed negligible thickness for electrodes. We have studied two cases in this paper, one with a small grounded electrode and the other with a long grounded electrode. The powered electrode extends from $x=1.7$ cm to

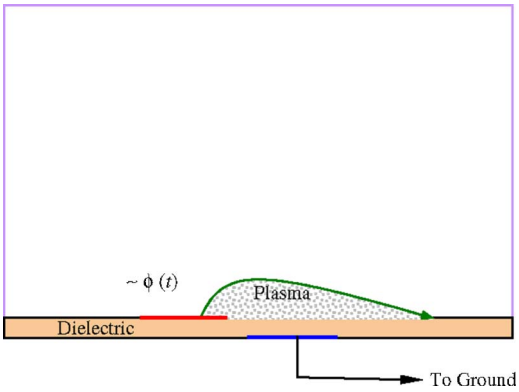

FIG. 1. (Color online) Schematic of asymmetric single dielectric barrier plasma actuators operating in air.

$x=1.9$ cm at $y=0.1$ cm for each case, the grounded electrode is from 2.1 to 2.3 cm for small grounded electrode case, and from 2.1 to 3.1 cm for long grounded electrode case. The grounded electrode is at $y=0$, with a 0.2 cm gap between rf and grounded electrodes along the x axis for both the cases. An alternating voltage of $\phi=1000\sin(10\,000\pi t)$ V is applied to the exposed electrode.

III. AIR CHEMISTRY

For the air chemistry we neglect the metastable species along with N^{4+} and O^{4+} due to their extremely high recombination rates. Also, the numerical complexity is further simplified by excluding nitrous oxide at this stage. The model equations governing chemistry of discharge are as follows.[12]

(1) Nitrogen model:

$$\text{Ionization } e + N_2 \rightarrow N_2^+ + 2e, \tag{1a}$$

$$\text{dissociation } e + N_2 \rightarrow 2N + e, \tag{1b}$$

$$\text{dissociative recombination } e + N_2^+ \rightarrow N_2. \tag{1c}$$

(2) Oxygen model:

$$\text{Ionization } e + O_2 \rightarrow O_2^+ + 2e, \tag{2a}$$

$$\text{dissociation } e + O_2 \rightarrow 2O + e, \tag{2b}$$

$$\text{dissociative attachment } e + O_2 \rightarrow O_- + O, \tag{2c}$$

$$\text{recombination } O^- + O_2^+ \rightarrow O + O_2, \tag{2d}$$

$$\text{dissociative recombination } O + O^- \rightarrow O_2 + e. \tag{2e}$$

The drift-diffusion form of continuity and Poisson equations for the electrons, ions, and neutrals are as follows:

$$\frac{\partial n_e}{\partial t} + \nabla \cdot (n_e \mathbf{v}_e) = k_1 n_e n_{N_2} - k_3 n_e n_{N_2^+} + (k_5 - k_7) n_e n_{O_2} + k_9 n_e n_{O_2^+}, \tag{3}$$

$$\frac{\partial n_N}{\partial t} + \nabla \cdot (n_N \mathbf{v}_N) = 2k_2 n_e n_{N_2}, \tag{4}$$

$$\frac{\partial n_{N_2}}{\partial t} + \nabla \cdot (n_{N_2}\mathbf{v}_{N_2}) = -k_1 n_e n_{N_2} - k_2 n_e n_{N_2} + k_3 n_e n_{N_2^+}, \quad (5)$$

$$\frac{\partial n_{N_2^+}}{\partial t} + \nabla \cdot (n_{N_2^+}\mathbf{v}_{N_2^+}) = k_1 n_e n_{N_2} - k_3 n_e n_{N_2^+}, \quad (6)$$

$$\frac{\partial n_{O_2}}{\partial t} + \nabla \cdot (n_{O_2}\mathbf{v}_{O_2}) = -(k_4 + k_5 + k_6) n_{O_2} n_e + k_7 n_{O^-} n_{O_2^+} + k_8 n_e n_{O_2^+}, \quad (7)$$

$$\frac{\partial n_O}{\partial t} + \nabla \cdot (n_O \mathbf{v}_O) = (2k_5 + k_6) n_e n_{O_2} + k_7 n_{O^-} n_{O_2^+}, \quad (8)$$

$$\frac{\partial n_{O^-}}{\partial t} + \nabla \cdot (n_{O^-}\mathbf{v}_{O^-}) = k_6 n_e n_{O_2} - k_7 n_{O^-} n_{O_2^+}, \quad (9)$$

$$\frac{\partial n_{O_2^+}}{\partial t} + \nabla \cdot (n_{O_2^+}\mathbf{v}_{O_2^+}) = k_4 n_e n_{O_2} - k_7 n_{O^-} n_{O_2^+} - k_8 n_e n_{O_2^+}, \quad (10)$$

$$\nabla \cdot (\varepsilon \nabla \phi) = 4\pi e (n_e + n_{O^-} - n_{N_2^+} - n_{O_2^+}), \quad (11)$$

with momentum flux $n_\alpha \mathbf{v}_\alpha = -\mathrm{sgn}(e) n_\alpha \mu_\alpha \nabla\phi - D_\alpha \nabla n_\alpha$, and electric field $\mathbf{E} = -\nabla\phi$. The electron temperature is calculated from $\mathbf{E} = k_B T_e / (\nabla n_e / n_e)$, which is obtained assuming an initial Boltzmann distribution, $n_e \propto \exp(e\phi / k_B T_e)$. Various rate coefficients $k_1, k_2, \ldots, k_8$ related to in Eqs. (1a)–(1c) and (2a)–(2e) are obtained from Kossyi *et al.*[12] as functions of electron temperature. The secondary electron emission from the exposed surface is taken as a function of incident electron energy[13] and remains small, i.e., less than 10^{-3}. No material sputtering of the surface is considered. In Eqs. (3)–(11), n_α and $\mathbf{v}_\alpha$ are density and velocities of species α. The mobilities μ_α and diffusion rates D_α are taken from Ellis *et al.*[14] The bulk density of the air is taken to be 1.3 $\mathrm{kg/m^3}$. Atmospheric ratio of 3.6 is taken for nitrogen to oxygen gas molecules.

IV. NUMERICAL DETAILS

The self-consistent formulation is solved using a Galerkin variational formulation based finite element method to obtain electron, ion, and neutral species densities of nitrogen and oxygen, and the electric potential. The details of the numerical procedures are given in our earlier work.[15] An adaptive time step size was taken with the smallest step of one-hundredth of the dielectric relaxation time scale. Also for this problem, we used the smallest element thickness of the order of Debye length about the powered electrode.

Initial and boundary conditions are as follows. The all initial particle concentrations, except those of the electrons, nitrogen, and oxygen molecules, are taken to be zero. Initial oxygen molecule density is taken as $10^{26}/\mathrm{m^3}$ nitrogen density is taken as $3.6\times10^{26}/\mathrm{m^3}$, and the electron density is taken as $10^4/\mathrm{m^3}$. Initial rf potential is also zero. These initial conditions have been chosen to match with near atmospheric conditions. The solution will be sensitive to the initial conditions; however, we report the results for the initial conditions chosen.

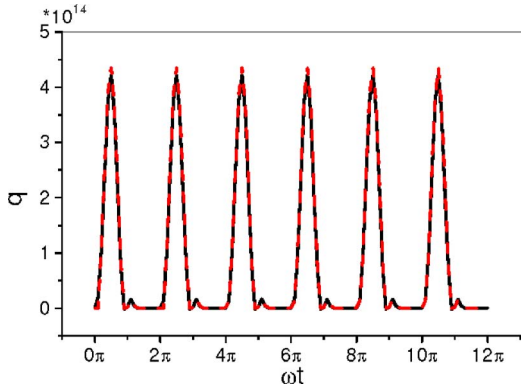

FIG. 2. (Color online) Temporal evolution of charge separation q as a function of normalized time ωt at $x=1.9$ cm and $y=1.1$ mm. The dashed line is for short grounded electrode and the solid line is for long grounded electrode.

Boundary conditions for Poisson's equation are as follows: The potential is applied to the exposed electrode with $\phi = 1000 \sin(10\,000\pi t)$ V. The embedded electrode is grounded. Electric insulation condition (normal component of electric field equal to zero) is assumed at outer boundaries of the domain. Electric field normal to the dielectric surface is discontinuous by the separated charge.

Boundary conditions related to air species continuity equations are as follows: the currents flow normal only to the rf electrode since it is an equipotential surface. Homogeneous Neumann conditions are applied to the outer edges of the domain and electric insulation is assumed at the surface of the dielectric. The currents flow normal as well as parallel to the dielectric surface.

V. RESULTS AND DISCUSSION

Discharge in the air starts as we switch on the rf voltage. Different ion and neutral species are formed through ionization, dissociation, dissociative attachment, etc. Recombination also occurs. Full chemistry of different species formation and recombination is described by Eq. (1) and (2). The simulation results at the tenth cycle are given in Figs. 2–8.

Figure 2(a) shows variation of charge separation $n_q = n_{O_2^+} + n_{N_2^+} - n_e - n_{O^-}$ as a function of normalized time ωt for $x=1.9$ cm and $y=1.1$ mm. Steady state is reached within a few cycles. The highest value of charge separation is near positive peaks of the cycles. The values of charge separation are nearly $4.2\times10^{14}/\mathrm{m^3}$ for small grounded electrode case and nearly $4.4\times10^{14}/\mathrm{m^3}$ for long grounded electrode case.

Figures 3(a) and 3(b) show spatial distribution of electron density for small grounded electrode and long grounded electrode. Chemistry of electron formation is given by the set of Eqs. (1) and (2). Spatial and temporal density profile of electrons is governed by continuity equation (3) coupled with other equations. Electron densities grow to a level $8\times10^{14}/\mathrm{m^3}$ for small grounded electrode case and nearly $7\times10^{14}/\mathrm{m^3}$ for long grounded electrode case. Electrons respond to electric field very fast due to low mass and high

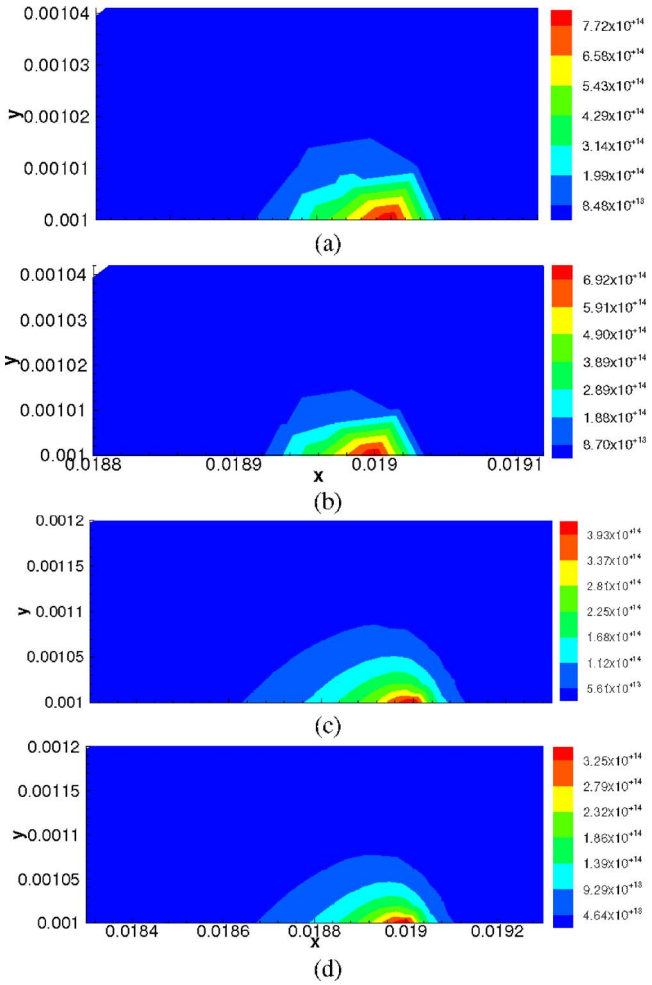

FIG. 3. (Color online) Spatial profiles of electron and O^- density for small and long grounded electrodes.

mobility. The electrons are repelled from the area near the grounded electrode and are attracted towards rf electrode during the positive part of the cycle. Reverse would happen during the negative part of the cycle. The oxygen ions O^- are produced through dissociative attachment of oxygen molecules with electrons governed by Eq. (2c). Its density is governed by continuity equation (9) coupled with other equations. Densities of oxygen ions O^- grow to a level of nearly $4\times10^{14}/m^3$ for small grounded electrode case and nearly $3.5\times10^{14}/m^3$ for long grounded electrode case. Figures 3(c) and 3(d) show density profile of negative oxygen ions O^- at the positive peak of the tenth cycle. The negative oxygen ions play an important role in oxygen chemistry. The oxygen ions O^- are repelled from the area of grounded electrode and are attracted towards rf electrode during the positive part of the cycle. The oxygen ions O^- are much heavier than that of electrons and its mobility is low; response is slow. Figures 4(a) and 4(b) show electron and negative oxygen ion densities, respectively, as a function of x for small and long grounded electrode cases. The tip of rf electrode is at $x=1.9$ cm. The peak of density is slightly before the tip of the rf electrode. Electric field direction and negative charge of these species are responsible for this location of densities. Density decreases sharply with the increase in the value of y. Electron and negative oxygen ion peak density is much higher for small grounded electrode than that for long grounded electrode.

The nitrogen atoms are produced through dissociation given by Eq. (1b) and its density is governed by continuity equation (4) coupled with other equations. Figures 5(a) and 5(b) show distribution of nitrogen atom density at positive peaks of the tenth cycle for small grounded electrode and long grounded electrode. The density of nitrogen atoms grows to a level of nearly $1.5\times10^{16}/m^3$ for both small grounded electrode case and long grounded electrode case. Since nitrogen atoms do not have any charge, no electric force works on these atoms. Their dynamic response time is very slow and these remain nearly at the same location where produced. The distribution is symmetric with respect to the x axis. The oxygen atoms are produced through dissociation of oxygen molecules given by Eq. (2b). The chemistry of oxygen atom formation is governed by Eq. (8) and its density is governed by continuity equation (14) coupled with other equations. Figures 5(c) and 5(d) show density profile of oxygen atom O at the positive peak of the cycle for small grounded electrode and long grounded electrode. The density of oxygen atoms grows to a level of nearly $3.5\times10^{16}/m^3$ for both small grounded electrode case and long grounded electrode case. The density of oxygen atoms is higher than that of nitrogen atoms due to the difference in rate coefficients related to the formation of nitrogen and oxygen atoms. Density profiles of both nitrogen and oxygen atoms are similar to each other because both are neutral atoms, do not respond to electric field, and remain at the location of production. The

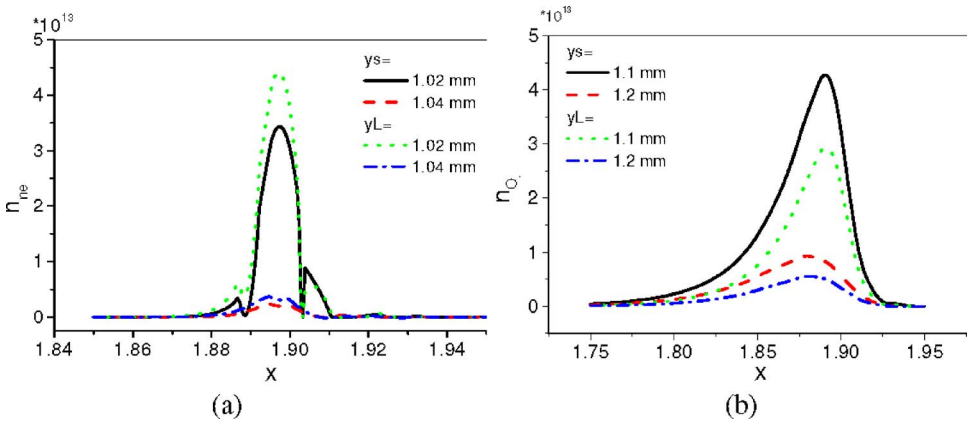

FIG. 4. (Color online) The electron and O^- density (m^{-3}) as a function of x for small (ys) and long (yL) grounded electrode cases. Here x is in cm.

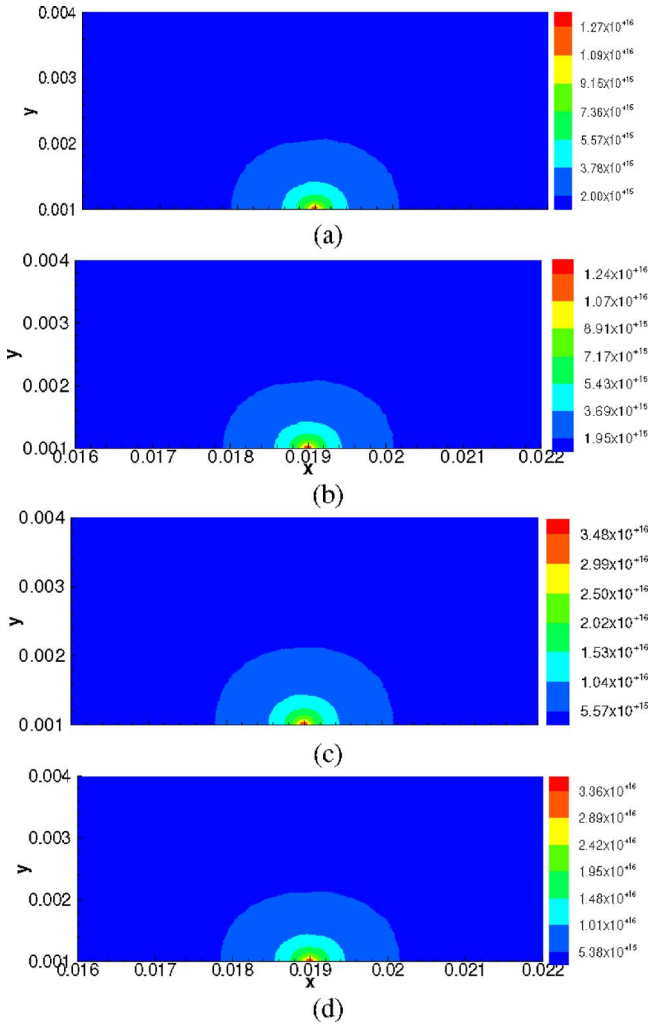

FIG. 5. (Color online) Spatial profiles of densities (m^{-3}) of N and O atoms for small and long grounded electrodes.

highest density of these neutral atoms is in between the two electrodes. Peak densities of nitrogen and oxygen atoms are higher than that of other species because these neutral species do not move from the location of production due to electric field.

The nitrogen ions N_2^+ are produced through ionization of nitrogen molecules given by Eq. (1a). Its density is governed by continuity equation (6) coupled with other equations. Figures 6(a) and 6(b) show distribution of nitrogen ion density $n_{N_2^+}$ at the positive peak of the tenth cycle for small grounded electrode and long grounded electrode cases, respectively. The density of nitrogen ions N_2^+ grows to nearly $8 \times 10^{14}/m^3$ for both small grounded electrode case and long grounded electrode case. The oxygen ions O_2^+ are produced through ionization of oxygen molecules. Chemistry of oxygen ion O_2^+ formation is given by Eq. (4) and its density is governed by continuity equation (10) coupled with other equations. The density of oxygen ions O_2^+ grows to nearly $3 \times 10^{13}/m^3$ for both small grounded electrode case and long grounded electrode case. Figures 6(c) and 6(d) show distribution of oxygen ion density O_2^+ at the positive peak of the tenth cycle for small grounded electrode and long grounded electrode, respectively. The N_2^+ and O_2^+ respond to electric field in a similar manner; hence, their density profiles are

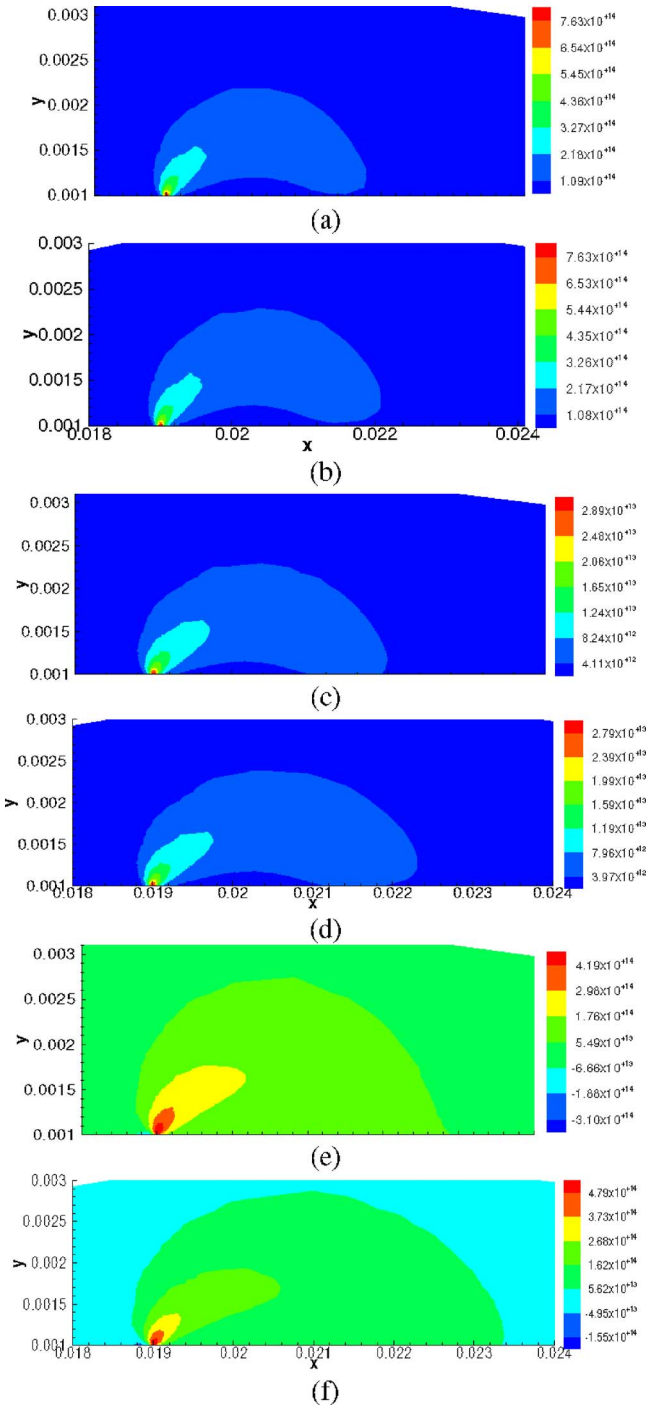

FIG. 6. (Color online) Spatial distributions of densities (m^{-3}) of N_2^+, O_2^+ and charge separation q for small and long grounded electrodes.

similar to each other. The peak of ion density is observed very close to the corner of rf electrode near the dielectric surface. The nitrogen and oxygen ions are concentrated in the sheath region about the electrodes. The difference between density levels of nitrogen and oxygen is because of the ratio of parent gas molecules in atmospheric air and difference in rate coefficients. The nitrogen ions are repelled from the area of rf electrode and are attracted towards grounded electrode during the positive part of the cycle. The response of negative ions to electric field is opposite to that of positive ions. Ion mass and motilities are different for different air species; hence their velocities are different. This gives rise to

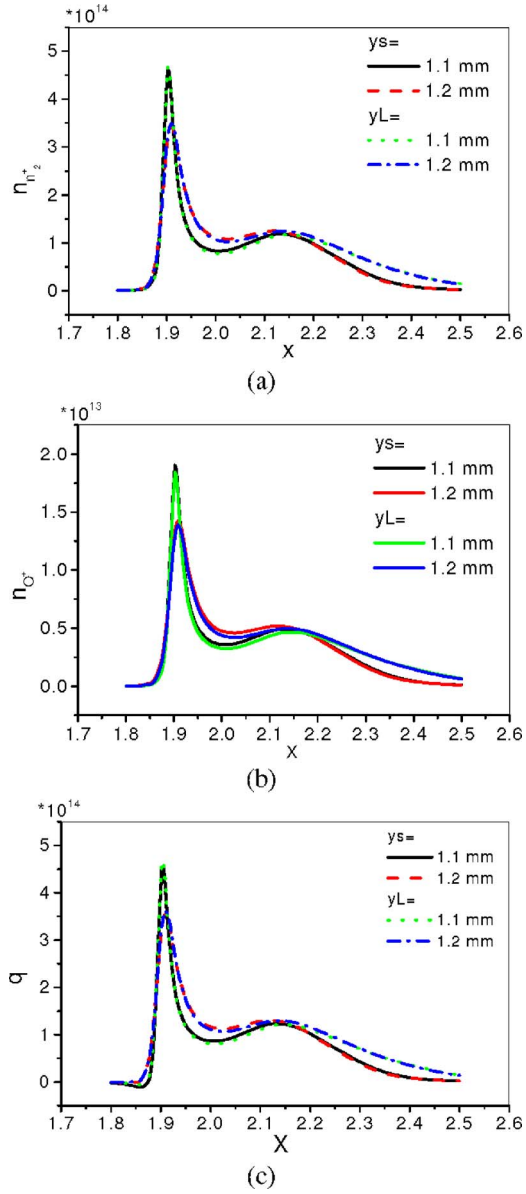

FIG. 7. (Color online) The N_2^+, O_2^+ and q density (m^{-3}) as a function of x for small (ys) and long (yL) grounded electrodes. Here x is in cm.

charge separation $n_q = n_{O_2^+} + n_{N_2^+} - n_e - n_{O^-}$. Figures 6(e) and 6(f) show density profile of charge separation at the positive peak of the tenth cycle for small grounded electrode and long grounded electrode, respectively. It resembles that of density profiles of positive nitrogen and oxygen ions. The value of charge separation q is nearly equal to the density of N_2^+ ions and electrons because densities of other charge species such as O^- and O_2^+ are small in comparison. The charge separation gives rise to a self-generated electric field through Poisson's equation. Figures 7(a)–7(c) show positive nitrogen ion, positive oxygen ion, and charge separation densities, respectively, as a function of x for both small and long grounded electrodes. The peak of density is very close to the tip of the rf electrode. The strength and direction of electric field and charge of these species are responsible for this location of densities. The density decreases sharply with the increase in the value of y. The peak ion densities are comparable for small grounded electrode than that for long grounded electrode. The direction of electric field changes with the increase in the length of grounded electrode in such a way that the density of species increases downstream.

Figure 8 shows spatial distributions of vectors of time average of electrodynamic force for small (in the left) and long (in the right) grounded electrode cases. We have given the vectors of time averaged force due to positive ions (a1, b1), negative species (a2, b2), and then due to all charged particles (a3, b3). The average force due to the negative ions is small as compared to that due to the negative ions and is in the opposite direction over the cycle. Thus the effective time averaged force due to all the charged species is smaller than that due to positive ions alone. The force is strong between two electrodes due to high electric field. A larger submerged electrode leads to an increase in the x component of electric field and leads to a larger volume discharge (see Ref. 4, Fig. 20). The magnitude of force that is higher during the positive part of the cycle is higher than that during the negative part of the cycle; hence, the net force is in the positive x direction. The direction of force is from rf electrode to grounded electrode. The magnitude of electrodynamic force is *slightly higher* for the long electrode case than that for the short electrode case. The magnitude of the y component of force decreases and the x component increases with the increase in the length of grounded electrode. The x component of force increases which will translate to a small increase in velocity. This trend also matches with reported experimental results.[4] The time averaged force is always positive and pushes the bulk air in the forward direction.

VI. CONCLUSIONS

Air discharge has been studied using an asymmetric dielectric barrier plasma actuator. A self-consistent plasma actuator model is employed to study surface discharge of air. Chemistry of formation of different ion and neutral species of nitrogen and oxygen has been taken into account. Species with very high recombination rates and nitrous oxide have been neglected for simplicity. Continuity equations governing densities of electrons, ions, and neutral species of nitrogen and oxygen are solved with Poisson's equation using a two-dimensional finite element based formulation of plasma to obtain spatial and temporal profiles of densities and voltage. Oppositely charged species move in the opposite directions due to applied driver rf potential which gives rise to charge separation. Poisson's equation governs electric field generated due to charge separation. The response of electrons to electric field is very fast as compared to ions due to small mass and high mobility of electrons. Density profiles of nitrogen atoms and oxygen atoms are symmetric to the x axis and are similar to each other because these do not respond to electric field. Density profiles of N_2^+ and O_2^+ are similar to each other at the positive peak of the cycle because both respond to electric field in a similar manner. There is, however, difference in the level of ionization of different species due to difference in density of parent air molecules and rate coefficients. The values of charge separation $n_q = (n_{O_2^+} + n_{N_2^+} - n_e - n_{O^-})$ and the electrodynamic force per volume $\mathbf{F} = e(n_{N_2^+} + n_{O_2^+} - n_e - n_{O^-})\mathbf{E}$ have been obtained. The average force due to the negative ions is small as compared to that

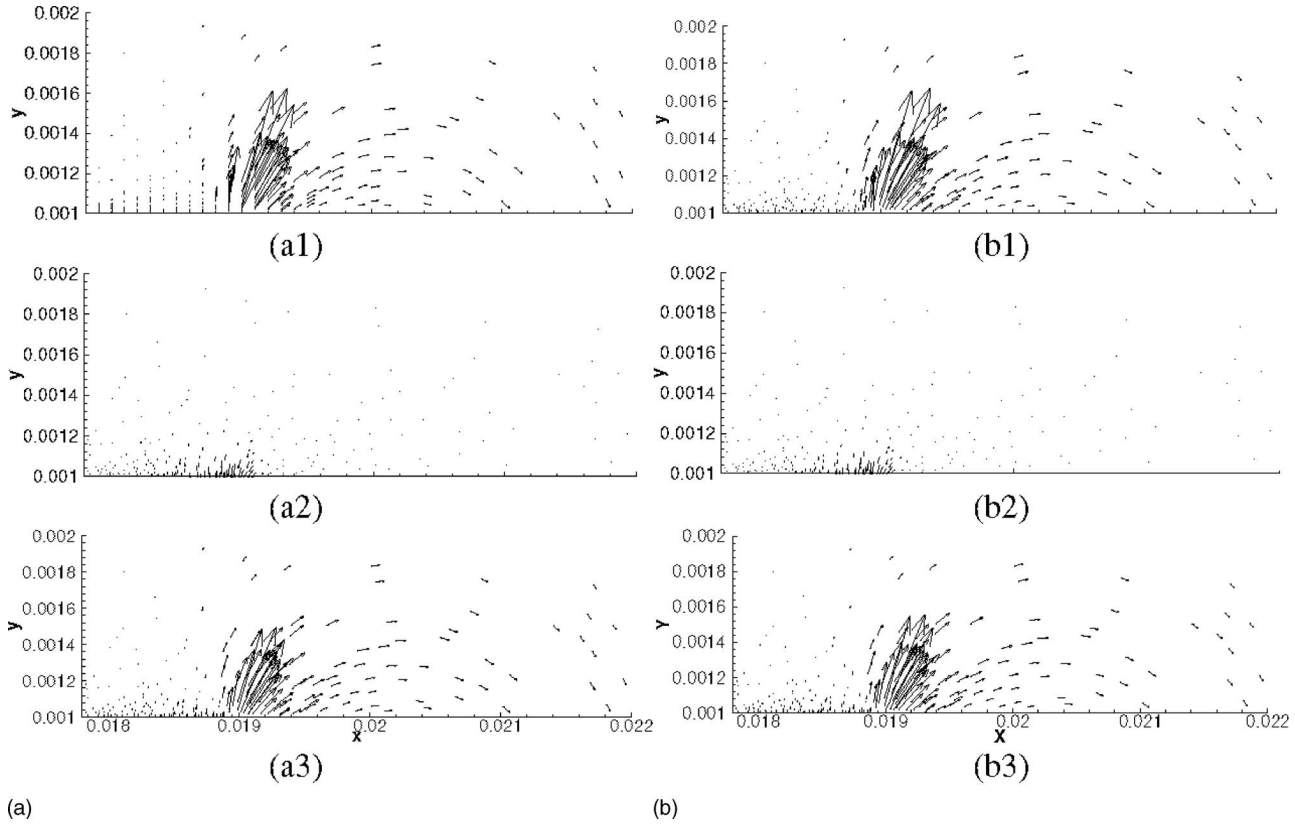

FIG. 8. Spatial distributions of vectors of time average of electrodynamic force for (a) small and (b) long grounded electrodes.

due to the negative ions and is in the opposite direction. The total average force due to all the charged species is smaller than that due to positive ions alone. The time average of the force is in the positive x direction over the domain; therefore, there is an average net force on the plasma in the positive x direction. This will result in a moving wave of plasma over the dielectric surface in the positive x direction which can find application in flow control. We have also investigated effect of change in length of grounded electrode on density profiles of species and on electrodynamic force. Electric field profile changes with the increase in grounded electrode and the density downstream increases. The magnitude of the force slightly increases with the increase in the length of grounded electrode but more investigation is needed to verify the trend for very large grounded electrode.

ACKNOWLEDGMENTS

This work was partially supported by the AFOSR Grant No. FA9550-05-1-0074 monitored by Lt. Col. Rhett Jefferies and the Air Force Research Laboratory Contract No. F33615-98-D-3210 and the National Academy of Science NRC/AFOSR and AFRL research fellowships during the past summers. The authors acknowledge thoughtful discussions with Drs. Datta Gaitonde and Miguel Visbal.

[1]J. P. Bons, R. Sondergard, and R. B. Rivir, J. Turbomach. **123**, 198 (2001); C. L. Enloe, T. E. McLaughlin, R. D. Van Dyken, K. D. Kachner, E. J. Jumper, T. C. Corke, M. Post, and O. Haddad, AIAA J. **42**, 595 (2004); T. C. Corke and M. L. Post, 43rd Aerospace Sciences Meeting, Reno, NV, 2005 (AIAA, Washington, D.C., 2002), Paper No. AIAA-2005-0563.

[2]J. R. Roth, Phys. Plasmas **10**, 2117 (2003); L. S. Hultgren and D. E. Ashpis, Bull. Am. Phys. Soc. **47**(10), 167 (2002).

[3]S. Roy, Appl. Phys. Lett. **86**, 101502 (2005); S. Roy and D. V. Gaitonde, 43rd Aerospace Sciences Meeting, Reno, NV, 2005 (AIAA, Washington, D.C., 2002), Paper No. AIAA-2005-0160; 35th AIAA Fluid Dynamics Conference and 36th AIAA Plasma Dynamics and Laser Conference, Toronto, Canada, June 2005 (AIAA, Washington, D.C., 2002), Paper No. AIAA-2005-4631.

[4]J. R. Roth and X. Dai, 44th AIAA Aerospace Sciences Meeting and Exhibit, Reno, NV, 9–12 January 2006 (AIAA, Washington, D.C., 2002), Paper No. AIAA-2006-1203.

[5]S. Roy, K. P. Singh, H. Kumar, D. V. Gaitonde, and M. Visbal, 44th AIAA Aerospace Sciences Meeting and Exhibit, Reno, NV, 9–12 January 2006 (AIAA, Washington, D.C., 2002), Paper No. AIAA-2006-0374; K. P. Singh, S. Roy, and D. Gaitonde, Plasma Sources Sci. Technol. **15**, 735 (2006).

[6]C. Baird, C. L. Enloe, T. E. McLaughlin, and J. W. Baughn, 43rd Aerospace Sciences Meeting, Reno, NV, 2005 (AIAA, Washington, D.C., 2002), Paper No. AIAA-2005-0565.

[7]W. Shyy, B. Jayaraman, and A. Anderson, J. Appl. Phys. **92**, 6434 (2002); D. M. Orlov, T. C. Corke, and M. P. Patel, AIAA 44th Aerospace Sciences Meeting, Reno, NV, 2006 (AIAA, Washington, D.C., 2002), Paper No. AIAA-2006-1202.

[8]S. Roy and D. V. Gaitonde, J. Appl. Phys. **96**, 2476 (2004); D. V. Gaitonde, M. R. Visbal, and S. Roy, 36th AIAA Plasmadynamics and Laser Conference, Toronto, Canada, June 2005 (AIAA, Washington, D.C., 2002), Paper No. AIAA-2005-5302; K. P. Singh and S. Roy, J. Appl. Phys. **98**, 083303 (2005); A. V. Likhanskii, M. N. Shneider, S. O. Macheret, and R. B. Miles, 44th AIAA Aerospace Sciences Meeting, Reno, NV, 2006 (AIAA, Washington, D.C., 2002), Paper No. AIAA-2006-1204.

[9]M. Visbal, D. Gaitonde, and S. Roy, Fluid Dynamics and Flow Control Conference, San Francisco, CA, June 2006 (AIAA, Washington, D.C., 2002), Paper No. AIAA-2006-3230; D. V. Gaitonde, M. R. Visbal, and S. Roy, 44th Aerospace Sciences Meeting, Reno, NV, 2006 (AIAA, Washington, D.C., 2002), Paper No. AIAA-2006-1205.

[10]G. Font, L. Enloe, T. Mclaughlin, and D. Orlov, 45th AIAA Aerospace Sciences Meeting and Exhibit, Reno, NV, 2007 (AIAA, Washington, D.C., 2002), Paper No. AIAA-2007-188.

[11]K. P. Singh, S. Roy, and D. Gaitonde, Fluid Dynamics and Flow Control Conference, San Francisco, CA, June 2006 (AIAA, Washington, D.C., 2002), Paper No. AIAA-2006-3381; S. Roy, K. P. Singh, and D. Gaitonde,

45th AIAA Aerospace Sciences Meeting and Exhibit, Reno, NV, 2007 (AIAA, Washington, D.C., 2002), Paper No. AIAA-2007–0184.
[12]I. A. Kossyi, A. Yu Kostinsky, A. A. Matveyev, and V. P. Silakov, Plasma Sources Sci. Technol. **1**, 207 (1992).
[13]S. Roy and B. P. Pandey, Phys. Plasmas **9**, 4052 (2002).
[14]H. W. Ellis, R. Y. Pai, E. W. McDaniel, E. A. Mason, and L. A. Viehland, At. Data Nucl. Data Tables **17**, 177 (1976).
[15]S. Roy and D. Gaitonde, Phys. Plasmas **13**, 023503 (2006).